Silhouette Coherence for Camera Calibration under Circular Motion

Carlos Hernández, Francis Schmitt and Roberto Cipolla

Abstract

We present a new approach to camera calibration as a part of a complete and practical system to recover digital copies of sculpture from uncalibrated image sequences taken under turntable motion. In this paper we introduce the concept of the *silhouette coherence* of a set of silhouettes generated by a 3D object. We show how the maximization of the silhouette coherence can be exploited to recover the camera poses and focal length.

Silhouette coherence can be considered as a generalization of the well known epipolar tangency constraint for calculating motion from silhouettes or outlines alone. Further, silhouette coherence exploits all the information in the silhouette (not just at epipolar tangency points) and can be used in many practical situations where point correspondences or outer epipolar tangents are unavailable.

We present an algorithm for exploiting silhouette coherence to efficiently and reliably estimate camera motion. We use this algorithm to reconstruct very high quality 3D models from uncalibrated circular motion sequences, even when epipolar tangency points are not available or the silhouettes are truncated. The algorithm has been integrated into a practical system and has been tested on over 50 uncalibrated sequences to produce high quality photo-realistic models. Three illustrative examples are included in this paper. The algorithm is also evaluated quantitatively by comparing it to a state-of-the-art system that exploits only epipolar tangents.

Index Terms

Silhouette coherence, epipolar tangency, image-based visual hull, camera motion and focal length estimation, circular motion, 3d modeling.

I. INTRODUCTION

Computer vision techniques are becoming increasingly popular for the acquisition of high quality 3D models from image sequences. This is particularly true for the digital archiving of cultural heritage, such as museum objects and their 3D visualization, making them available to people without physical access.

Recently, a number of promising multi-view stereo reconstruction techniques have been presented that are now able to produce very dense and textured 3D models from calibrated images. These are typically optimized to be consistent with stereo cues in multiple images by using space carving [1], deformable meshes [2], volumetric optimization [3], or depth maps [4].

The key to making these systems practical is that they should be usable by a non-expert in computer vision such as a museum photographer, who is only required to take a sequence of high quality still photographs. In practice, a particularly convenient way to acquire the photographs is to use a circular motion or turntable setup (see Fig. 1 for two examples), where the object is rotated in front of a fixed, but uncalibrated camera. Camera calibration is thus a major obstacle in the model acquisition pipeline. For many museum objects, between 12 and 72 images are typically acquired and automatic camera calibration is essential.

Among all the available camera calibration techniques, point-based methods are the most popular (see [5] for a review and [6] for a state-of-the-art implementation). These rely on the presence of feature points on the object surface and can provide very accurate camera estimation results. Unfortunately, especially in case of man-made objects and museum artifacts, feature points are not always available or reliable (see the example in Fig. 1b). For such sequences, there exist alternative algorithms that use the object outline or silhouette as the only reliable image feature, exploiting the notion of epipolar tangents and frontier points [7]–[9] (see [10] for a review). In order to give accurate results, these methods require very good quality silhouettes, making their integration in a practical system difficult. For the particular case of turntable motion, the silhouette segmentation bottleneck is the separation of the object from the turntable. A common solution is to clip the silhouettes (see example in Fig. 1b). Another instance of truncated silhouettes occurs when acquiring a small region of a bigger object (see Fig. 1a).

We present a new approach to silhouette-based camera motion and focal length estimation that exploits the notion of multi-view *silhouette coherence*. In brief, we exploit the rigidity property of 3D objects to impose the key geometric constraint on their silhouettes, namely that there must exist a 3D object that could have generated these silhouettes. For a given set of silhouettes and camera projection matrices, we are able to quantify the agreement of both the silhouettes and the projection matrices, i.e, how much of the silhouettes could have been generated by a real object given those projection matrices. Camera estimation is then seen as an optimization step where silhouette coherence is treated as a function of the camera matrices that has to be **maximized**. The proposed technique extends previous silhouette-based methods and can deal with partial or truncated silhouettes, where the estimation and matching of epipolar tangents can be very difficult or noisy. It also exploits more information than is available just at epipolar tangency points. It is especially convenient when combined with 3D object modeling techniques that already fuse silhouettes with additional cues, as in [2], [3], [11].

This paper is organized as follows: in Section II we review the literature. In Section III we state our problem formulation. In Section IV we introduce the concept of silhouette coherence. In Section V we describe the actual algorithm for camera calibration. In Section VI we illustrate the accuracy of the method and show some high quality reconstructions.

II. Previous work

Many algorithms for camera motion estimation and auto-calibration have been reported [5]. They typically rely on correspondences between the same features detected in different images. For the particular case of circular motion, the methods of [12] and [13] work well when the images contain enough texture to allow a robust detection of their features. An alternative is to exploit silhouettes. Silhouettes have already been used for camera motion estimation using the notion of *epipolar tangency points* [7], [8], [14], *i.e.*, points on the silhouette contours in which the tangent to the silhouette is an epipolar line. A rich literature exists on exploiting epipolar tangents, both for orthographic cameras [7], [9], [15], [16] and perspective cameras [17]–[20]. In particular, the works of [18] and [19] use only the two outermost epipolar tangents, which eliminates the need for matching corresponding epipolar tangents across different images. Although these methods have given good results, their main drawback is the limited number of epipolar tangency points per pair of images, generally only two: one at the top and one at the bottom of the silhouette. When additional epipolar tangency points are available, the goal is to match them across different views and handle their visibility, as proposed in [16] and [20].

(a)

(b)

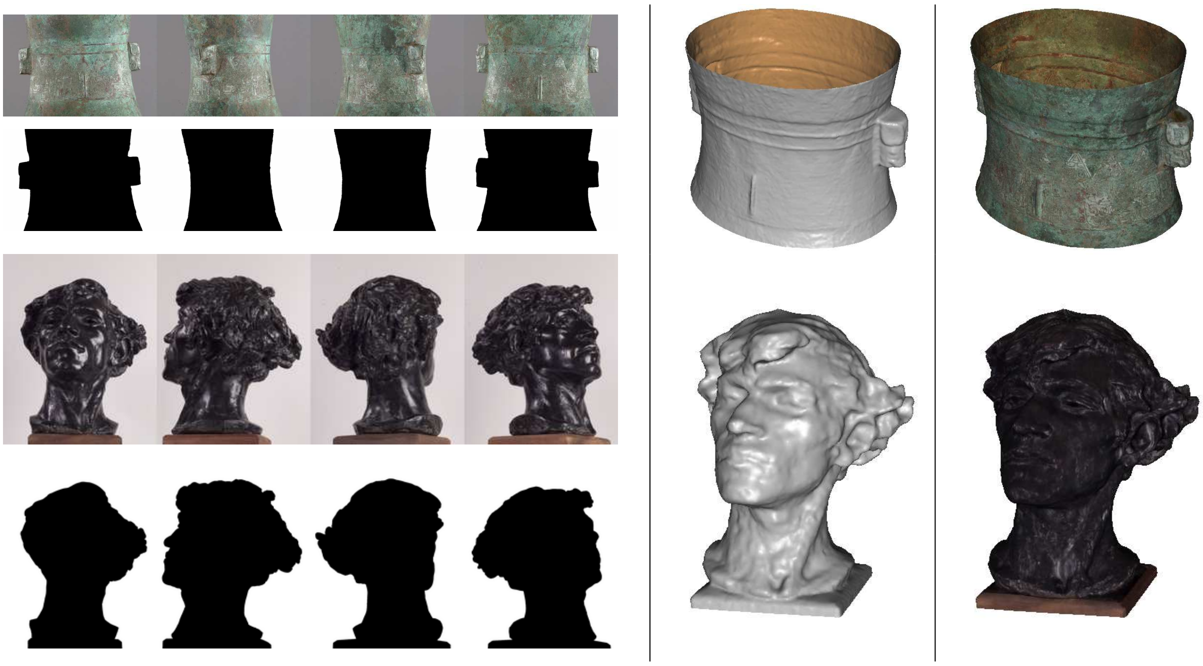

Fig. 1. Reconstructed sculptures after camera motion and focal length estimation using silhouette coherence. (a) Chinese bronze vase (24 input images of 6 Mpixels). (b) Giganti by Camille Claudel (36 input images of 6 Mpixels). Left bottom: corresponding segmented silhouettes. Middle: reconstructed shaded model. Right: textured model.

An additional limitation of all these methods is their inability to cope with partial or truncated silhouettes, as in the examples shown in Fig. 1.

Although the notion of silhouette coherence appears in the literature under different names, it has never been exploited before for camera estimation. Bottino and Laurentini study the problem of *silhouette compatibility* in [21] for the case of orthographic projection, and give some rules to determine if a set of silhouettes can correspond to a real object. They do not provide a way to quantify the amount of *incompatibility*. In his PhD thesis, Cheung [22] used the phrase *consistent alignment* for the idealized registration of two visual hulls. However, in practice, his proposal was not feasible in an optimization algorithm because it was too computationally expensive. In this paper we further develop the concept of silhouette coherence and link it to the epipolar geometry, and specifically to the tangency criterion as used by Wong and Cipolla [19]. In particular, the epipolar tangency criterion can be seen as a measure of silhouette coherence for the special case of only two silhouettes. When using more than two silhouettes, the proposed silhouette coherence extends the epipolar tangency criterion by exploiting all the information contained in the contours of the silhouettes, not just at the epipolar tangency points. This enables us to estimate the motion and the focal length correctly even if there are no epipolar tangents available (see Fig. 1a). The proposed silhouette coherence criterion is also related to [23], where silhouette coherence is used to register a laser model with a set of images. The main difference with this paper is that we do not require a 3D representation of the object in order to perform camera calibration. The object is *implicitly* reconstructed from the silhouettes by a visual hull method at the same time as the cameras are calibrated.

III. Problem formulation

We consider a perspective projection camera model where the relation between a 3D point $\mathbf{M}$ and its 2D projection $\mathbf{m}$ is fully represented by the 3×4 camera projection matrix P [5]:

$$\mathbf{m} \simeq \mathsf{P}\mathbf{M} \simeq \mathsf{K}[\mathsf{R}|\mathbf{t}]\mathbf{M}, \tag{1}$$

where the 3×3 rotation matrix R and the vector $\mathbf{t}$ represent the orientation and translation defining the pose of the camera. The calibration matrix K contains the intrinsic parameters of the camera. The aspect ratio and the skew factor are assumed to be known or ideal for our CMOS and CCD cameras; the only intrinsic parameters that we consider are the focal length f (in pixels) and the principal point $(u_0, v_0)^\top$. Furthermore, since the effect of the translation $\mathbf{t}$ and the principal point $(u_0, v_0)^\top$ is very similar under the assumption of circular motion, the principal point is considered to simply be the center of the image.

For n views, we parameterize the circular motion with $n+3$ parameters[1] (see Fig. 2b): the spherical coordinates of the rotation axis $(\theta_\mathbf{a}, \phi_\mathbf{a})$, the translation direction angle $\alpha_\mathbf{t}$, the $n-1$ camera angle steps $\Delta\omega_i$ and the focal length f. The i^{th} camera projection matrix P_i has the following decomposition:

$$\mathsf{P}_i = \mathsf{K}[\mathsf{R}_i|\mathbf{t}_i] = \mathsf{K}[\mathsf{R}_\mathbf{a}(\omega_i)|\mathbf{t}] \;\forall i, \tag{2}$$

where $\mathsf{R}_\mathbf{a}(\omega_i)$ is the rotation of angle ω_i around axis $\mathbf{a}$ and the vectors $\mathbf{a}$ and $\mathbf{t}$ are given as:

$$\begin{aligned} \mathbf{a} &= (\sin(\theta_\mathbf{a})\cos(\phi_\mathbf{a}), \sin(\theta_\mathbf{a})\sin(\phi_\mathbf{a}), \cos(\theta_\mathbf{a}))^\top, \\ \mathbf{t} &= (\sin(\alpha_\mathbf{t}), 0, \cos(\alpha_\mathbf{t}))^\top. \end{aligned} \tag{3}$$

[1]We could also have used the parameterization of [12] instead.

(a)

(b)

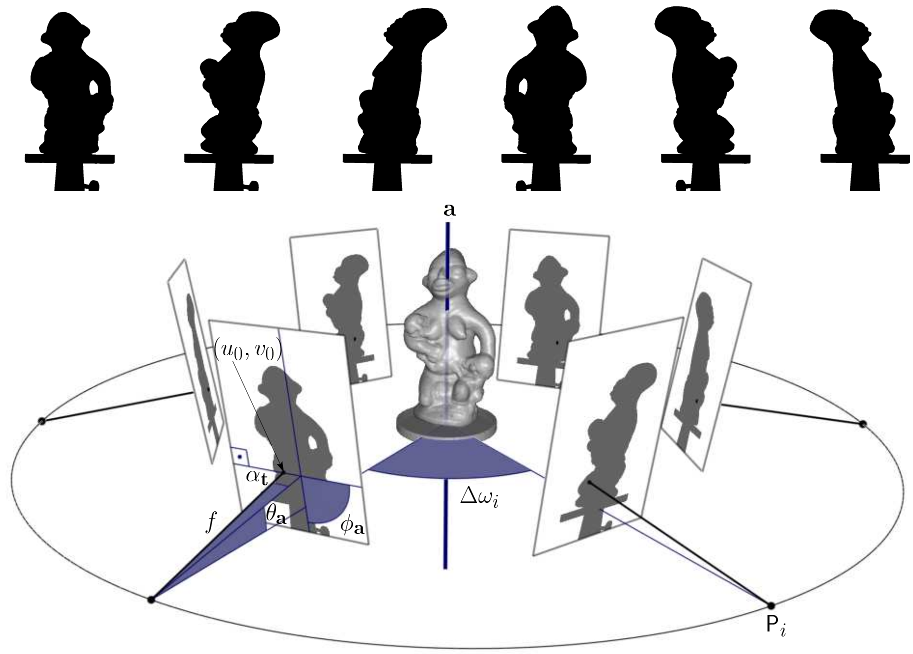

Fig. 2. Circular motion parameterization. (a) Set of input silhouettes S_i. (b) Parameterization of the projection matrices P_i as a function of the spherical coordinates of the rotation axis $(\theta_{\mathbf{a}}, \phi_{\mathbf{a}})$, the translation direction $\alpha_{\mathbf{t}}$, the camera angle steps $\Delta\omega_i$ and the focal length f.

Given a set of silhouettes S_i of a rigid object taken under circular motion (see Fig. 2a), our goal is to recover the corresponding projection matrices P_i as the set of $n+3$ parameters $\mathbf{v} = (\theta_{\mathbf{a}}, \phi_{\mathbf{a}}, \alpha_{\mathbf{t}}, \Delta\omega_i, f)$ (see Fig. 2b).

IV. Silhouette coherence

Given a set of silhouettes S_i of the same 3D object, taken from different points of view, and a corresponding set of camera projection matrices P_i, we would like to measure the agreement of both the silhouette segmentation and the camera projection matrices. We want to exploit the raw information provided by a silhouette: a binary classification of all the optic rays going through the optic center of the associated camera. These optic rays are labeled by the silhouette as *intersecting the object* (**S** label) if they belong to a silhouette pixel, or **not** *intersecting the object* (**B** label) if they belong to a background pixel.

Let us consider an optic ray defined by a silhouette pixel and thus classified as **S**. The projection of the optic ray into any other view *must* intersect the corresponding silhouette. Furthermore,

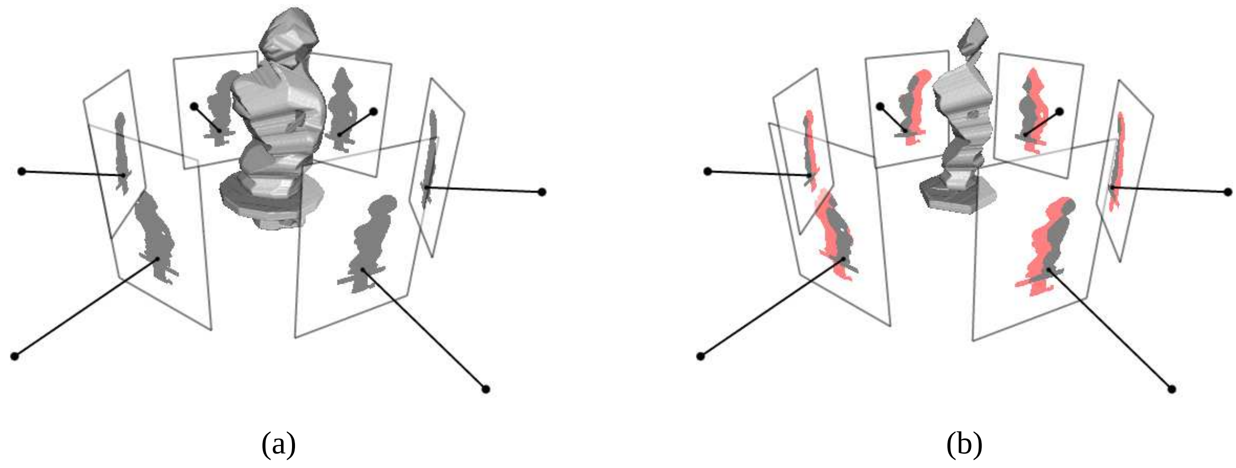

Fig. 3. Two examples of different degrees of silhouette coherence. The reconstructed visual hull $\mathcal{V}$ is shown by the gray 3D object. (a) A perfectly coherent silhouette set. (b) Same set of silhouettes with a different pose and low silhouette coherence. The red area shows non-coherent silhouette pixels. In this paper we minimize the red area as a criterion for camera calibration (see video in supplemental material).

the back projection of all these 2D intersection intervals onto the optic ray *must* be **coherent**, meaning that their intersection must have non-zero length. The intersection interval will contain the exact position where the optic ray touches or intersects the object.

Due to noisy silhouettes or incorrect camera projection matrices, the above statement may not be satisfied, *i.e.*, even if a silhouette has labeled an optic ray as **S**, its depth interval might be empty. In the case of only two views, the corresponding silhouettes will not be coherent if there exists at least *one* optic ray classified as **S** by one of the silhouettes whose projection does not intersect the other silhouette. In the case of n views, the lack of coherence is defined by the existence of at least one optic ray where the depth intervals defined by the $n-1$ other silhouettes have an empty intersection. This lack of coherence can be measured simply by counting how many optic rays in each silhouette are not coherent with the other silhouettes. Two examples of coherent and non-coherent silhouettes are shown in Fig. 3. The silhouette pixels that are not coherent with the other silhouettes are shown in red in Fig. 3b.

A simple way of measuring the silhouette coherence using the concept of visual hull [24] is as follows:

- compute the reconstructed visual hull defined by the silhouettes and the projection matrices,
- project the reconstructed visual hull back into the cameras, and

- compare the reconstructed visual hull silhouettes with the original silhouettes.

In the situation of ideal data, *i.e.*, perfect segmentation and exact projection matrices, the reconstructed visual hull silhouettes and the original silhouettes will be exactly the same (see Fig. 3a). With real data, both the silhouettes and the projection matrices will be imperfect. As a consequence, the original silhouettes and the reconstructed visual hull silhouettes will not be the same, the latter silhouettes being **always contained** in the original ones (see Fig. 3b).

A. A robust measure of silhouette coherence

Let $\mathcal{V}$ be the visual hull defined by the set of silhouettes S_i and the set of projection matrices P_i, and $S_i^{\mathcal{V}}$ its projection into the i^{th} image. A choice must be made about how to measure the similarity $\mathcal{C}$ between the silhouette S_i and the projection of the reconstructed visual hull $S_i^{\mathcal{V}}$. A quick answer would be to use the ratio of areas between these two silhouettes as in [23]:

$$\mathcal{C}(S_i, S_i^{\mathcal{V}}) = \frac{\int S_i^{\mathcal{V}}}{\int S_i} = \frac{\int (S_i \cap S_i^{\mathcal{V}})}{\int S_i} \in [0, 1]. \tag{4}$$

However, this measure has the major disadvantage of a very high computation cost, as mentioned by [22]. To address this important issue, we propose a simple replacement in (4) of the silhouette S_i by its contour, C_i:

$$\mathcal{C}(S_i, S_i^{\mathcal{V}}) = \frac{\int (C_i \cap S_i^{\mathcal{V}})}{\int C_i} \in [0, 1]. \tag{5}$$

This new measure is much faster than (4) since, as discussed in Section V, we propose to discretize the evaluation of the measure. Hence, the computation time of (5) is proportional to the **length** term $(C_i \cap S_i^{\mathcal{V}})$, while the computation time of (4) is proportional to the **area** term $(S_i \cap S_i^{\mathcal{V}})$. However, a possible weakness concerning the use of the contour instead of the silhouette itself is that these two measures might differ for some problematic cases as shown in Fig. 4b and Fig. 4c. The contour-based measure will penalize the Fig. 4b scenario, while encouraging scenarios such as Fig. 4c. If none of the silhouettes has interior holes, the latter is impossible by virtue of how the visual hull is constructed. Case b, however, is much more common for the problem of silhouette coherence and can be easily reproduced if one of the silhouettes is dilated due to a segmentation error.

In order to alleviate this limitation of using contours instead of areas for case b, we propose a δ-offset silhouette contour approach (see Fig. 5). For a given δ value we replace in (5) the

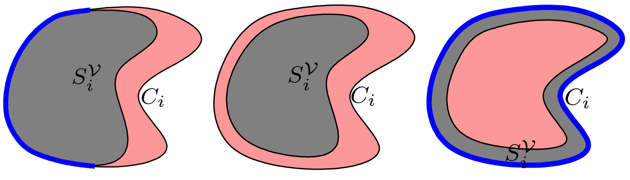

(a) (b) (c)

Fig. 4. Limitation of using contours for silhouette comparison. The silhouette of the visual hull $S_i^{\mathcal{V}}$ is shown in dark gray and the difference with S_i is shown in red. The intersection $C_i \cap S_i^{\mathcal{V}}$ is drawn with a thick blue stroke. (a) Ideal scenario; using contours and areas is equivalent. (b) Problematic case where the coherence using contours is much lower (0 in this example) than when using areas. (c) Problematic case with a hole in the silhouette $S_i^{\mathcal{V}}$. The coherence using contours is much higher (1 in this example) than when using areas.

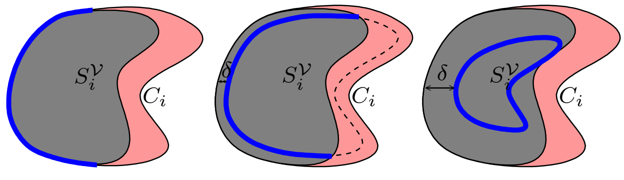

$\mathcal{C}^\delta = 0.4$ $\mathcal{C}^\delta = 0.7$ $\mathcal{C}^\delta = 1$

Fig. 5. Avoiding the limitation of using contours for silhouette comparison. From left to right, increasing δ values imply increasing silhouette coherence values and better robustness for scenario of Fig. 4b. The original silhouette S_i corresponds to the outermost contour. The silhouette of the reconstructed visual hull $S_i^{\mathcal{V}}$ is shown in dark gray. The term $(C_i \ominus \delta) \cap S_i^{\mathcal{V}}$ in (6) is shown with a thick blue stroke.

contour C_i by its eroded version of δ pixels $C_i \ominus \delta$, which gives:

$$\mathcal{C}^\delta(S_i, S_i^{\mathcal{V}}) = \frac{\int((C_i \ominus \delta) \cap S_i^{\mathcal{V}})}{\int(C_i \ominus \delta)} \in [0, 1]. \tag{6}$$

Increasing δ makes the new measure more robust against bad segmentation. But robustness is obtained at the price of accuracy. For a given δ value, the silhouette coherence will not be able to distinguish between a silhouette S_i and its reconstructed visual hull silhouette $S_i^{\mathcal{V}}$ if their difference is smaller than δ. Typical values of δ range from 0.25 pixels to several pixels, depending on the quality of the silhouette segmentation.

Equation (6) evaluates the *coherence* between the silhouette S_i and all the other silhouettes $S_{j \neq i}$ that contributed to the reconstructed visual hull. In fact, since $S_i^{\mathcal{V}}$ is fully determined by the silhouette contours $C_{j=1,\cdots,n}$, equation (6) can also be noted as $\mathcal{C}^\delta(C_i, C_{j=1,\cdots,n})$, or $\mathcal{C}^\delta(C_i, C_{j \neq i})$. To compute the total coherence between all the silhouettes, we simply compute the average coherence between each silhouette and the $n-1$ others:

$$\mathcal{C}^\delta(C_1, \ldots, C_n) = \frac{1}{n} \sum_{i=1}^{n} \mathcal{C}^\delta(C_i, C_{j \neq i}) \in [0, 1]. \tag{7}$$

B. *Relation to epipolar geometry and epipolar tangents*

The proposed silhouette coherence criterion can be seen as an extension to methods based on epipolar tangency points. For a given pair of views, as shown in Fig. 6, the epipolar tangency

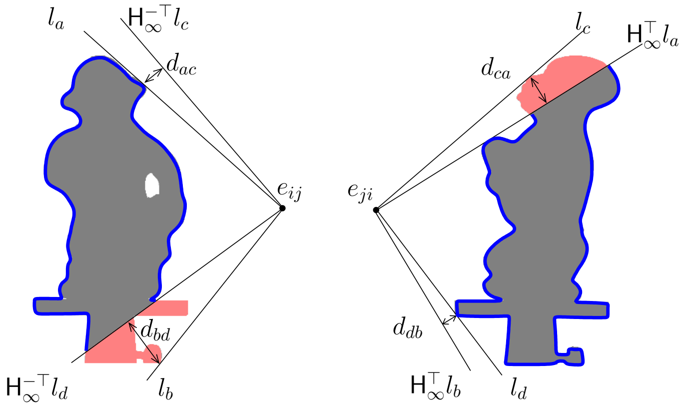

Fig. 6. Epipolar tangency and silhouette coherence criteria for $n = 2$ silhouettes. The silhouettes of the visual hull $S_i^{\mathcal{V}}$ and $S_j^{\mathcal{V}}$ are shown in dark gray. The terms $C_i \cap S_i^{\mathcal{V}}$ and $C_j \cap S_j^{\mathcal{V}}$ are drawn with a thick blue stroke. Both criteria are equivalent for the case of 2 views: they minimize the sectors defined by l_b and $\mathsf{H}_\infty^{-\top} l_d$, and l_c and $\mathsf{H}_\infty^{\top} l_a$ (shown in red).

approach minimizes the square distance between epipolar tangents of one view (l_a and l_b in view i, l_c and l_d in view j) and the transferred epipolar tangents of the other view via the fundamental matrix $\mathsf{F}_{ij} = [e_{ij}]_\times \mathsf{H}_\infty$ ($\mathsf{H}_\infty^{-\top} l_c$ and $\mathsf{H}_\infty^{-\top} l_d$ in view i, $\mathsf{H}_\infty^{\top} l_a$ and $\mathsf{H}_\infty^{\top} l_b$ in view j). That is, it minimizes the sum of geometric distances $\mathcal{C}_{et}(C_i, C_j) = d_{ac}^2 + d_{bd}^2 + d_{ca}^2 + d_{db}^2$. For the same pair of silhouettes, the optimization of the coherence criterion corresponds to maximizing the lengths $C_i \cap S_i^{\mathcal{V}}$ and $C_j \cap S_j^{\mathcal{V}}$. So we can see that, except for degenerate configurations, both criteria try to minimize the sectors defined by the epipolar tangents in one view and their corresponding epipolar tangents in the other view. Thus, if we optimize our coherence criterion taking the silhouettes in pairs, we get the same behavior as with methods based on epipolar tangents, *e.g.* [19].

When using the proposed silhouette coherence for $n > 2$, silhouettes are not just taken in pairs but all at the same time. This means that the information we exploit is not just at the epipolar tangency points but all over the silhouette contour. As a result, even if we use silhouettes where the epipolar tangents are not available, the silhouette coherence criterion is still valid. We present an example in Fig. 1a where we do not have the top and the bottom of the silhouettes (no outer epipolar tangents available) but for which we are still able to estimate the motion and the focal length with very good accuracy.

It is worth noting that, as mentioned by [22], maximizing silhouette coherence is a *necessary condition* but not a *sufficient* one in order to recover camera motion. However, since silhouette coherence is an extension of epipolar tangency criteria, the same limitation applies to previous methods using epipolar tangency points. If silhouette coherence is optimized, so is the epipolar tangency criterion. This can be checked easily in Fig. 6. In practice, maximizing silhouette coherence is sufficient and can be used for camera calibration, as demonstrated by the reconstruction of more than 50 sequences (available for download at [25]) obtained using the 3D modeling technique described in [2]. In order to use the modeling algorithm, cameras were calibrated using the technique described in this paper.

V. Overview of the camera estimation algorithm

We now present a practical implementation of the silhouette coherence criterion $\mathcal{C}^\delta$, achieved by discretizing the contour $C_i \ominus \delta$ into a number of equally spaced sample points. The term $(C_i \ominus \delta) \cap S_i^{\mathcal{V}}$ is evaluated by testing, for each sample point, if its associated optic ray intersects the reconstructed visual hull using a ray casting technique [26]. A simplified version of this algorithm is used, where we do not take into account contours inside the silhouettes. Furthermore, we do not compute all the depth intervals for a given optic ray. We just compute the minimum and maximum of the interval intersection with each silhouette. This is a conservative approximation of the real coherence, *i.e.*, the coherence score that we obtain by storing only the minimum and maximum depths is always equal or greater than the real one. However, in practice, the deviation from the coherence computed with all the intervals is small.

The algorithm describing the silhouette coherence $\mathcal{C}^\delta(C_i, C_{j\neq i})$ between a given silhouette contour C_i and the remaining silhouette contours $C_{j\neq i}$ is shown in Algorithm 1. If N is the number of sample points per silhouette, and n is the number of silhouettes, the complexity of $\mathcal{C}^\delta(C_i, C_{j\neq i})$ is $\mathcal{O}(nN\log(N))$. The total silhouette coherence $\mathcal{C}^\delta(C_i, \ldots, C_n)$ in (7) is shown in Algorithm 2 and its complexity is $\mathcal{O}(n^2 N \log(N))$. As an example, the computation time of one evaluation of (7) on an Athlon 1.5 GHz processor is 750 ms for the Pitcher example of Fig. 7 ($n = 18$, $N \approx 6000$).

In order to exploit silhouette coherence for camera motion and focal length estimation under circular motion, the **key** is to use the silhouette coherence as the **cost** in an optimization procedure. Equation 7 can be seen as a "*black box*" that takes as input a set of silhouettes and projection matrices, and gives as output a scalar value of silhouette coherence. We use Powell's derivative-free optimization algorithm [27] to maximize (7). Several hundred cost evaluations

Algorithm 1 Silhouette coherence $\mathcal{C}^\delta(C_i, C_{j\neq i})$

Require: Projection matrices P_i $\forall i$, reference contour C_i, contour list $C_{j\neq i}$, contour offset δ, number of samples per contour N

Build point list $\mathbf{m}^{(k)}$, sampling N points along $C_i \ominus \delta$

for all $\mathbf{m}^{(k)}$ **do**

  Initialize 3D interval $I_{3D} = [0, \infty]$

  Initialize counter $N' = 0$

  for all $C_{j\neq i}$ **do**

    Project optic ray $l = \mathsf{P}_j \mathsf{P}_i^{-1} \mathbf{m}^{(k)}$

    Compute 2D intersection interval $I_{2D} = l \cap C_j$

    Back project 2D interval $I_{3D} = I_{3D} \cap \mathsf{P}_j^{-1} I_{2D}$

  end for

  if $I_{3D} \neq \emptyset$ **then**

    $N' = N' + 1$

  end if

end for

Return $\frac{N'}{N}$

Algorithm 2 Total silhouette coherence $\mathcal{C}^\delta(C_{i=1,\cdots,n})$

Require: Sequence of contours $C_{i=1,\cdots,n}$, camera parameters $\mathbf{v} = (\theta_\mathbf{a}, \phi_\mathbf{a}, \alpha_\mathbf{t}, \Delta\omega_i, f)$

Compute P_i from $\mathbf{v}$ using (2) and (3).

Return average $\frac{1}{n}\sum_{i=1}^{n} \mathcal{C}^\delta(C_i, C_{j\neq i})$ {Algorithm 1}

Algorithm 3 Motion and focal length estimation

Require: Sequence of images $I_{i=1,\cdots,n}$

Extract contours C_i from I_i (*e.g.* [28]),

Initialize $\mathbf{v} = (\theta_\mathbf{a}, \phi_\mathbf{a}, \alpha_\mathbf{t}, \Delta\omega_i, f)$=($\frac{\pi}{2}, \frac{\pi}{2}, 0, \frac{2\pi}{n}, f_0$),

Initialize Powell's derivative-free algorithm [27]

repeat {see [27] for details}

  $\mathbf{v}' = \mathbf{v}$

  $\mathbf{v}$ = Powell($\mathbf{v}'$) {Single Powell iteration with Algorithm 2}

until $||\mathbf{v} - \mathbf{v}'|| < \epsilon$

are typically required before convergence.

The system is always initialized with the same default circular motion: the rotation axis $\mathbf{a} = (0,1,0)^\top$ ($\theta_\mathbf{a} = \frac{\pi}{2}$, $\phi_\mathbf{a} = \frac{\pi}{2}$), the translation $\mathbf{t} = (0,0,1)^\top$ ($\alpha_\mathbf{t} = 0$) and the initial guess of the camera angles (*e.g.*, $\Delta\omega_i = \frac{2\pi}{n}$). The initial guess of the focal length f_0 is directly computed from typical values of the field of view, *e.g.*, 20 degrees. The principal point is considered constant and equal to the center of the image. The complete algorithm for motion and focal length estimation is described in Algorithm 3. Because circular motion is a very constrained motion, we have found that the initial values for the rotation axis, the translation direction and the focal length do not need to be very close to the actual solution. The only source of convergence problems is the initial camera angles, but the algorithm has proven to have good convergence properties for camera angle errors of up to 15 degrees.

VI. Experimental results

We present an experiment using a Pitcher sequence with 18 color images of 2008x3040 pixels acquired with a computer controlled turntable. The images have been segmented by an automatic procedure [28] (see Fig. 7). For evaluation we also use a sequence of a calibration pattern in

Fig. 7. Pitcher sequence. Some of the original images superimposed with the extracted smooth polygon contours (in black).

Pitcher		rotation axis (degrees)		translation (degrees)	focal (pixels)
		$\theta_{\mathbf{a}}$	$\phi_{\mathbf{a}}$	$\alpha_{\mathbf{t}}$	f
initial		90.0000	90.0000	0.0000	5000
calibrated		99.671	90.3431	0.4266	6606
$\mathcal{C}_{et}$	recovered	99.6345	90.3050	0.4314	6576
	error	0.0364	0.0381	0.0049	30
$\mathcal{C}$	recovered	99.6861	90.3419	0.4239	6635
	error	0.0152	0.0011	0.0026	29

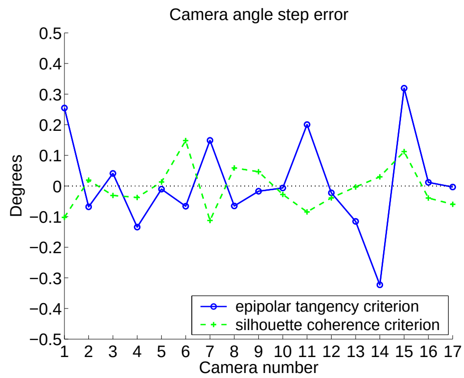

TABLE I

CAMERA ESTIMATION FOR THE PITCHER SEQUENCE. MEAN CAMERA ANGLE STEP ERROR OF 0.11 DEGREES USING EPIPOLAR TANGENCY POINTS ($\mathcal{C}_{et}$) AND 0.06 DEGREES USING SILHOUETTE COHERENCE ($\mathcal{C}$). NOTE THAT THE AXIS ERROR IS REDUCED BY A FACTOR OF 3, THE TRANSLATION ERROR BY A FACTOR OF 2, AND THE STEP ERROR BY A FACTOR OF 2.

order to accurately recover the intrinsic parameters and the circular motion using [29]. The δ-offset used for the silhouette coherence criterion is $\delta = 0.25$ pixels due to the sub-pixel accuracy of the silhouette extraction. The camera angles are initialized with a uniform random noise in the interval $[-15, 15]$ degrees around the true angles. We show in the supplemental video the initialization used in this example and how the different parameters are optimized by the silhouette coherence.

Table I contains the results for the camera motion (rotation axis, translation direction and camera angles) and focal length estimation problem. A total of 21 parameters are recovered. We compare the proposed silhouette coherence with the state-of-the-art method described in [19]. The silhouette coherence clearly outperforms [19] by reducing the rotation axis error by a factor of 3, the translation error by a factor of 2 and the camera angles error by a factor of 2. Both criteria recover the focal length with the same accuracy ($\sim 0.5\%$).

The same camera estimation algorithm has been repeatedly tested successfully on over 50 uncalibrated sequences. We illustrate in Fig. 1 two of these sequences that are particularly interesting. For the Chinese bronze vase (Fig. 1a) the two outermost epipolar tangents are not available, since the tops and bottoms of the silhouettes are truncated. For the Giganti sculpture (Fig. 1b) just the bottom has been truncated. Problems with correctly extracting the bottom of an object are common under turntable motion. In general, it is easy to extract the top of an object, but it is much more difficult to separate the bottom from the turntable. We validate the motion and calibration results by the quality of the final reconstructions, generated using an implementation of the algorithm described in [2]. Note that the Giganti sculpture (Fig. 1b) would be very difficult to calibrate using point-based techniques, its surface being very specular, while the Chinese vase (Fig. 1a) is impossible for epipolar tangent algorithms.

Two additional experiments ara available as supplemental material in appendix I. In the first experiment we compare the accuracy of the silhouette coherence and the epipolar tangency criteria as a function of silhouette noise. In the second experiment we show that silhouette coherence exploits more information that epipolar tangency points alone by showing that it can calibrate the cameras even when no epipolar tangency points are available.

VII. Conclusions and future work

A new approach to silhouette-based camera estimation has been developed. It is built on the concept of silhouette coherence, defined as a similarity between a set of silhouettes and the silhouettes of their visual hull. This approach has been successfully tested for the problem of circular motion. The high accuracy of the estimation results is due to the use of the full silhouette contour in the computation, whereas previous silhouette-based methods just use epipolar tangency points. The proposed method eliminates the need for epipolar tangency points and naturally copes with truncated silhouettes. Previous algorithms are completely dependant on clean silhouettes and epipolar tangency points. We have validated the proposed approach both qualitatively and quantitatively.

A limitation of our current silhouette coherence implementation is the discretization of the silhouette contours. To remove this source of sampling noise, a solution would compute the exact visual hull silhouettes as polygons and compare them with the original silhouettes. To compute the exact silhouette of the visual hull, we can proceed as in [30], using a ray casting technique.

We are currently extending the proposed approach to roughly circular motion and general motion, but special attention has to be paid to the initialization process to avoid local minima, less important for the case of circular motion.

REFERENCES

[1] K. N. Kutulakos and S. M. Seitz, "A theory of shape by space carving," *IJCV*, vol. 38, no. 3, pp. 199–218, 2000.

[2] C. Hernández and F. Schmitt, "Silhouette and stereo fusion for 3d object modeling," *CVIU*, vol. 96, no. 3, pp. 367–392, 2004.

[3] G. Vogiatzis, P. Torr, and R. Cipolla, "Multi-view stereo via volumetric graph-cuts," in *CVPR*, 2005.

[4] P. Gargallo and P. Sturm, "Bayesian 3d modeling from images using multiple depth maps," in *CVPR*, vol. II, 2005, pp. 885–891.

[5] R. I. Hartley and A. Zisserman, *Multiple View Geometry in Computer Vision*. Cambridge University Press, ISBN: 0521623049, 2000.

[6] D. Nistér, "An efficient solution to the five-point relative pose problem," *IEEE Trans. on PAMI*, vol. 26, no. 6, pp. 756–770, June 2004.

[7] J. H. Rieger, "Three dimensional motion from fixed points of a deforming profile curve," *Optics Letters*, vol. 11, no. 3, pp. 123–125, 1986.

[8] J. Porrill and S. B. Pollard, "Curve matching and stereo calibration," *Image and Vision Computing*, vol. 9, no. 1, pp. 45–50, 1991.

[9] P. Giblin, F. Pollick, and J. Rycroft, "Recovery of an unknown axis of rotation from the profiles of a rotating surface," *J.Optical Soc. America*, vol. 11A, pp. 1976–1984, 1994.

[10] R. Cipolla and P. Giblin, *Visual Motion of Curves and Surfaces*. Cambridge University Press, 2000.

[11] M. Lhuillier and L. Quan, "Surface reconstruction by integrating 3d and 2d data of multiple views," in *ICCV*, 2003, pp. 1313–1320.

[12] A. W. Fitzgibbon, G. Cross, and A. Zisserman, "Automatic 3D model construction for turn-table sequences," in *3D SMILE*, June 1998, pp. 155–170.

[13] G. Jiang, H. Tsui, L. Quan, and A. Zisserman, "Single axis geometry by fitting conics," in *ECCV*, vol. 1, 2002, pp. 537–550.

[14] R. Cipolla, K. Åström, and P. Giblin, "Motion from the frontier of curved surfaces," in *ICCV*, Cambridge, June 1995, pp. 269–275.

[15] B. Vijayakumar, D. Kriegman, and J. Ponce, "Structure and motion of curved 3d objects from monocular silhouettes," in *CVPR*, 1996, pp. 327–334.

[16] Y. Furukawa, A. Sethi, J. Ponce, and D. Kriegman, "Structure and motion from images of smooth textureless objects," in *ECCV 2004*, vol. 2, Prague, Czech Republic, May 2004, pp. 287–298.

[17] K. Åström, R. Cipolla, and P. Giblin, "Generalized epipolar constraints," *IJCV*, vol. 33, no. 1, pp. 51–72, 1999.

[18] P. R. S. Mendonça, K.-Y. K. Wong, and R. Cipolla, "Epipolar geometry from profiles under circular motion," *IEEE Trans. on PAMI*, vol. 23, no. 6, pp. 604–616, June 2001.

[19] K.-Y. K. Wong and R. Cipolla, "Reconstruction of sculpture from its profiles with unknown camera positions," *IEEE Trans. on Image Processing*, vol. 13, no. 3, pp. 381 – 389, 2004.

[20] S. N. Sinha, M. Pollefeys, and L. McMillan, "Camera network calibration from dynamic silhouettes," in *CVPR*, vol. 1, 2004, pp. 195–202.

[21] A. Bottino and A. Laurentini, "Introducing a new problem: Shape-from-silhouette when the relative positions of the viewpoints is unknown," *IEEE Trans. on PAMI*, vol. 25, no. 11, pp. 1484–1493, 2003.

[22] K. Cheung, "Visual hull construction, alignment and refinement for human kinematic modeling, motion tracking and rendering," Ph.D. dissertation, Carnegie Mellon University, 2003.

[23] H. Lensch, W. Heidrich, and H. P. Seidel, "A silhouette-based algorithm for texture registration and stitching," *J. of Graphical Models*, pp. 245–262, 2001.

[24] A. Laurentini, "The visual hull concept for silhouette based image understanding," *IEEE Trans. on PAMI*, vol. 16, no. 2, 1994.

[25] http://www.tsi.enst.fr/3dmodels/.

[26] W. Matusik, C. Buehler, R. Raskar, S. Gortler, and L. McMillan, "Image-based visual hulls," in *SIGGRAPH 2000*, 2000, pp. 369–374.

[27] M. Powell, "An efficient method for finding the minimum of a function of several variables without calculating derivatives," *Computer Journal*, vol. 17, pp. 155–162, 1964.

[28] C. Xu and J. L. Prince, "Snakes, shapes, and gradient vector flow," *IEEE Trans. on Image Processing*, pp. 359–369, 1998.

[29] J. M. Lavest, M. Viala, and M. Dhome, "Do we really need an accurate calibration pattern to achieve a reliable camera calibration?" in *ECCV*, vol. 1, 1998, pp. 158–174.

[30] J.-S. Franco and E. Boyer, "Exact polyhedral visual hulls," in *BMVC*, September 2003, pp. 329–338.